Tailoring the fracture response of two-phase network reinforced composites through irregularity

Chelsea Fox [a], Tommaso Magrini [b,*] , Chiara Daraio [a,*]

[a] *Division of Engineering and Applied Science, California Institute of Technology, Pasadena, CA 91125, USA*
[b] *Department of Mechanical Engineering, Eindhoven University of Technology, 5600MB Eindhoven, The Netherlands*

ARTICLE INFO

ABSTRACT

The mechanical behavior of composite materials is significantly influenced by their structure and constituent materials. One emerging class of composite materials is irregular network reinforced composites (NRC's), whose reinforcing phase is generated by a stochastic algorithm. Although design of the reinforcing phase network offers tailorable control over both the global mechanical properties, like stiffness and strength, and the local properties, like fracture nucleation and propagation, the fracture properties of irregular NRC's have not yet been fully characterized. This is because both the irregular reinforcing structure and choice of matrix phase material significantly affect the fracture response, often resulting in diffuse damage, associated with multiple crack nucleation locations. Here, we propose irregular polymer NRC's whose matrix phase has a similar stiffness but half the strength of the reinforcing phase, which allows the structure of the reinforcing phase to control the fracture response, while still forming and maintaining a primary crack. Across a range of network coordination numbers, we obtain J-integral and R-curve measurements, and we determine that low coordination polymer NRC's primarily dissipate fracture energy through plastic zone formation, while high coordination polymer NRC's primarily dissipate energy through crack extension. Finally, we determine that there are two critical length scales to characterize and tailor the fracture response of the composites across the coordination numbers: (i) the size of the plastic zone, and (ii) the size and geometry of the structural features, defined as the areas enclosed by the reinforcing network.

1. Introduction

Architected materials often draw inspiration from the structure of biological materials to achieve desirable properties such as high stiffness and strength (Fox et al., 2024; Jung et al., 2024; Zhang et al., 2021), good energy dissipation (Fox et al., 2024; Gu et al., 2017b; Li et al., 2024; Zhuang et al., 2023), and high fracture toughness (Dai et al., 2023; Dimas et al., 2013; Gu et al., 2017a; Jia and Wang, 2019; Jung et al., 2024; Magrini et al., 2023, Magrini et al., 2022, 2019). These bioinspired materials also often feature two or more phases (Espinosa et al., 2009; Gu et al., 2017a; Li et al., 2024; Libonati et al., 2019, 2014; Magrini et al., 2019), as biological materials are typically composite materials, such as bone (Keaveny et al., 2003; Launey et al., 2010; Magrini et al., 2021; Whitehouse, 1974) or nacre (Ackson et al., 1988; Meyers et al., 2008), with mechanical properties superior to that of their constitutive elements. Although most bioinspired composite materials feature repeating structural patterns (Gao et al., 2023; Gu et al., 2016; Li

et al., 2022; Magrini et al., 2022, 2019; Studart, 2012), many biological materials have a non-periodic structure (Jentzsch et al., 2024, 2022; Metzler et al., 2019; Studart, 2012), indicating that evolution may favor irregularity as a way to optimize function (Metzler et al., 2019).

To explore the role of irregularity, virtual growth algorithms (VGA) have been developed to imitate the stochastic growth process of biological material structures (Jia et al., 2024a; Liu et al., 2022). These algorithms generate a continuous irregular network by assembling a set of building blocks according to local connectivity rules, and studies have been conducted to determine the relationship between the structure and function of these networks (Jia et al., 2024a, 2024b; Liu et al., 2022), including for polymer composite materials (Fox et al., 2024; Magrini et al., 2023), whose reinforcing phase is generated by the VGA. It has been shown that controlling the average network coordination (Thorpe and Duxbury, 2002; Thorpe, 1983), defined as the number of branches in each building block, primarily influences the stiffness and strength of the materials (Fox et al., 2024; Jia et al., 2024a; Magrini et al., 2023;

---

* Corresponding authors.

E-mail addresses: t.magrini@tue.nl (T. Magrini), daraio@caltech.edu (C. Daraio).

Zhou et al., 2024), while controlling the connectivity rules determines the formation of specific structural features, defined as the areas enclosed by the reinforcing network (Fox et al., 2024; Magrini et al., 2023).

However, despite the large design space offered by the choice of building blocks and their connectivity rules, polymer composites reinforced by stiff irregular networks with a compliant matrix display the same fracture behavior (Magrini et al., 2023). Fracture begins with the nucleation of voids in the compliant matrix, similar to what is observed in ductile metals (Anderson, 2017), followed by bridging of the reinforcing phase, similar to what occurs in fiber reinforced composites (Chen et al., 1995; Khan, 2019; Nemat-Nasser and Hori, 1987; Sakai et al., 1991). During fracture bridging, the most extensible portions of the reinforcing phase deform in the direction of the applied load, until they undergo local yielding followed by sequential strut failure (Magrini et al., 2023). The sequential failure of the reinforcing phase causes the coalescence of the large-scale voids, leading to the overall loss of structural integrity in the composites (Magrini et al., 2023).

Previous efforts have shown how to nucleate and guide the fracture path (Magrini et al., 2023), but the fracture properties of irregular network reinforced composites have not yet been fully characterized. To better understand the role of the reinforcing phase during fracture, we generate centimeter-scale polymer composite materials (with millimeter scale features), whose matrix phase has a similar stiffness but half the strength of the reinforcing phase. This prevents the diffuse nucleation of voids across the sample and maintains a primary crack, making fracture characterization measurements possible, while still allowing the reinforcing phase to significantly influence the fracture response. Across a
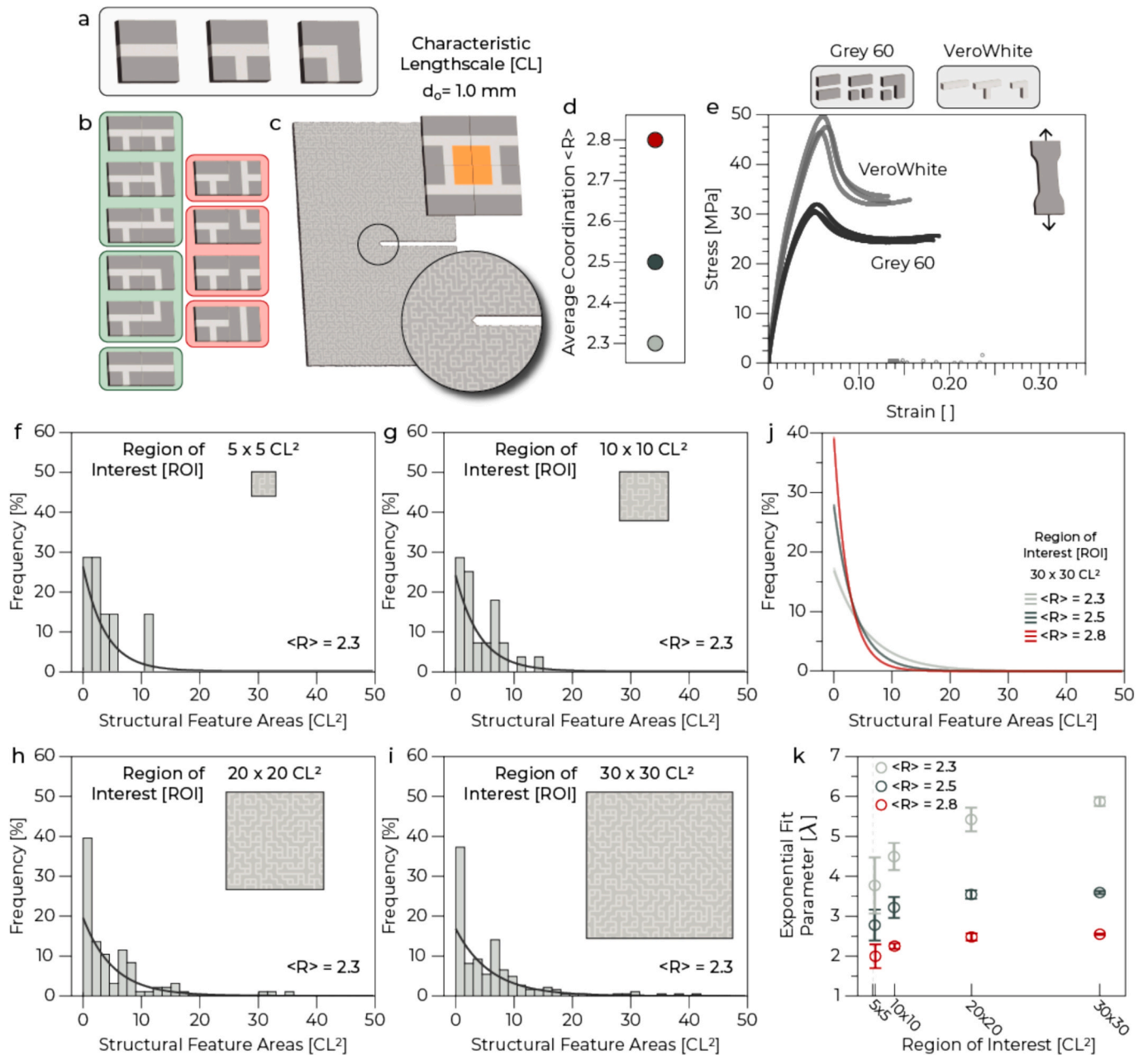

Fig. 1. Material and structural characterization. (a) VGA tiles and coordination numbers. (b) VGA connectivity rules, green is allowed, red is not allowed. (c) Fracture samples with characteristic length scale. (d) Average coordination number. (e) Constitutive uniaxial stress–strain plot for reinforcing and matrix phase materials. (f-i) Frequency of 2.3 coordination structural feature areas for 5x5, 10x10, 20x20 and 30x30 tiles. (j) Exponential fits of structural feature areas for 2.3, 2.5 and 2.8 coordination samples with 30x30 tiles. (k) Exponential fit parameters for increasing sizes of sample regions of interest.

range of coordinations from 2.3 to 2.8, we determine that there are two critical length scales necessary to understand and describe the fracture response of the composites: (i) the plastic zone size, and (ii) the structural feature size (and geometry). We then show how to tailor the tradeoff between plastic zone size and primary crack extension using the coordination number and its effect on the structural feature populations ahead of the crack tip.

2. Material and Methods

We generate the irregular reinforcing phase of the polymer composite samples using a VGA (Liu et al., 2022). This computer-assisted material design tool generates the irregular samples on a square grid from a set of three tile types, with coordination numbers of either two, for (−) tiles and (L) tiles, or three, for (T) tiles (Fig. 1a). Although the (−) and (L) tiles have the same coordination number, their geometry varies significantly, potentially influencing the mechanical properties. However, the (−) tiles represent a small fraction of the overall tile percentages used in this study and instead have a primary role of ensuring percolation in the VGA. Using tile frequency hints and a set of connectivity rules (Fig. 1b), the VGA assembles the tiles into continuous irregular networks (Fig. 1c), with a characteristic length defined as one tile, which is equivalent to the smallest possible structural feature that can be formed, with a size of 1 mm (Fig. 1c). We generate samples with an average coordination that ranges from 2.3 to 2.8 (Fig. 1d), which spans the transition from floppy to rigid behavior while maintaining percolation ("Rigidity Theory and Applications," 2002; Thorpe, 1983). The 2.3 coordination samples are composed of 5 % (−) tiles, 65 % (L) tiles and 30 % (T) tiles, the 2.5 coordination samples are composed of 5 % (−) tiles, 45 % (L) tiles and 50 % (T) tiles, and the 2.8 coordination samples are composed of 10 % (−) tiles, 10 % (L) tiles and 80 % (T) tiles, with equally represented two-fold ((−) tiles) or four-fold rotations ((L) and (T) tiles). To determine the sample size needed for testing, we determine the minimum number of tiles required for the network to be representative of the coordination number's population of structural features by finding an exponential fit and looking for when the exponential fit parameters converge as the sample size increases (Figs. 1j, 1k). We find that samples of 30x30 tiles are sufficiently representative (Figs. 1f-i), but we also note that networks with higher coordination reach a plateau more quickly than lower coordination ones, as the structural feature size depends on the coordination number (Fig. 1k).

To fabricate our polymer composite samples for single edge notch plate tension tests, we first choose the volume fraction of the reinforcing phase in each tile, with values of 20 % for 2-coordination tiles and 30 % for 3-coordination tiles, corresponding to a branch width of 0.2 mm. We then add a matrix phase with a similar stiffness (~1 GPa) (Dizon et al., 2018; Jia and Wang, 2019; Magrini et al., 2023; Slesarenko and Rudykh, 2018), but half the strength of the reinforcing phase (Fig. 1e) to fill the remaining space in each tile. We use a Polyjet printer (Stratasys Objet500 Connex3) to additively manufacture the composite materials using a commercially available photoresin (VeroWhite Polyjet Resin, Stratasys) for the reinforcing network, and a compatible photoresin with lower strength (Stratasys Grey60 Polyjet Resin) for the matrix (Fig. 1e). Furthermore, the composite materials have a strong adhesion between phases, key to avoid delamination during fracture testing, likely as a result of the low mismatch in mechanical properties of the two phases and simultaneous processing of both the matrix and reinforcing phase during additive manufacturing (Lumpe et al., 2019; Magrini et al., 2023; Nash and Li, 2021).

3. Results and Discussion

3.1. Single edge notch plate tension fracture tests

We conduct single edge notch plate tension fracture tests on composite samples of 9x6 cm, corresponding to 90x60 tiles (or characteristic lengths), with a thickness of 1 mm and an initial crack of length 3 cm, which we sharpen with a razor blade prior to testing. Grip areas of height 3 cm, manufactured from the same photoresin as the reinforcing phase, are added during printing to the top and bottom of the sample. We use an Instron E3000 (Instron, USA) equipped with a 5kN load cell to apply a tensile load at a rate of 2 mm/min and we test three different samples for each coordination, repeating one of these samples three times to verify that the same structure fractures self-consistently. We compare our results to samples exclusively composed of the matrix and reinforcing phases (Figs. 2a,e), and similar to the bulk materials, the composite samples maintain one primary crack, which initiates and propagates through both phases as the tensile loading is applied. This is the consequence of the relatively low mismatch in mechanical properties between the reinforcing and matrix phase polymers, which prevents crack arrest at the interface (Kolednik et al., 2014). Nonetheless, despite having similar volume fractions of reinforcing phase across the coordination numbers, with values of 23 %, 25 % and 28 % for 2.3, 2.5, and 2.8 coordinations, respectively, the force–displacement curves (Figs. 2b-d) display significant variations. Among composite samples, 2.3 coordination samples fail at the highest global strain, while 2.8 coordination samples fail at the lowest global strain (Figs. 2b,d). The measured strain-to-failure values are in between the recorded strain-to-failure values for the bulk materials (Figs. 2a,e). To explain these variations, we track the strain fields ahead of the crack tip using 2D digital image correlation. We spray the samples with matte white paint and apply matte black speckles of diameter 0.1–0.3 mm and then use VIC 2D (Correlated Solutions, USA) to analyze the Lagrangian strain fields. Unlike previous studies featuring composites with a soft elastomeric matrix, which are prone to multiple void nucleation sites and diffuse damage across the entire sample (Magrini et al., 2023) (Figure SI 1), we observe the formation of a single plastic zone across all samples. Assuming that plastic yielding begins when the maximum principal strain value exceeds the yield strain from the constitutive uniaxial stress–strain data, we apply a threshold and track the size of the plastic zone with respect to the sequential events: yield, crack initiation, and sample failure (Figs. 2f-j). Most importantly, we note that the plastic zone in all samples develops to be over one order of magnitude larger than the structural features.

3.2. Fracture behavior of the Composites: Plastic zone formation and crack extension

Although the plastic zone begins to develop at approximately the same global displacement in all samples, we observe that the maximum size of the plastic zone reached by each coordination increases nonlinearly with coordination number (Fig. 3a, SI 2). By tracking the amount of crack extension with respect to the global displacement applied, using the image processing software, FIJI (Schneider et al., 2012), we also observe that lower coordination samples have less crack extension despite reaching a higher global strain. Indeed, the 2.3 coordination samples do not exceed 1.4 ± 0.2 mm of crack extension, while 2.8 coordination samples reach up to 3.5 ± 0.8 mm of crack extension before their sudden failure (Fig. 3b). This tradeoff between plastic zone size, crack extension, and global strain-to-failure is also reflected in the J-integrals for each sample. We define the J-integral for an edge cracked sample as:

$$J = \frac{\eta U}{Bb} \#$$

(1)

where η is a dimensionless constant, U is the area under the force displacement curve, B is the sample thickness, and b is the uncracked length(Anderson, 2017) (Fig. 3b, inset). The J-integral can also be written as a sum of its elastic and plastic components:
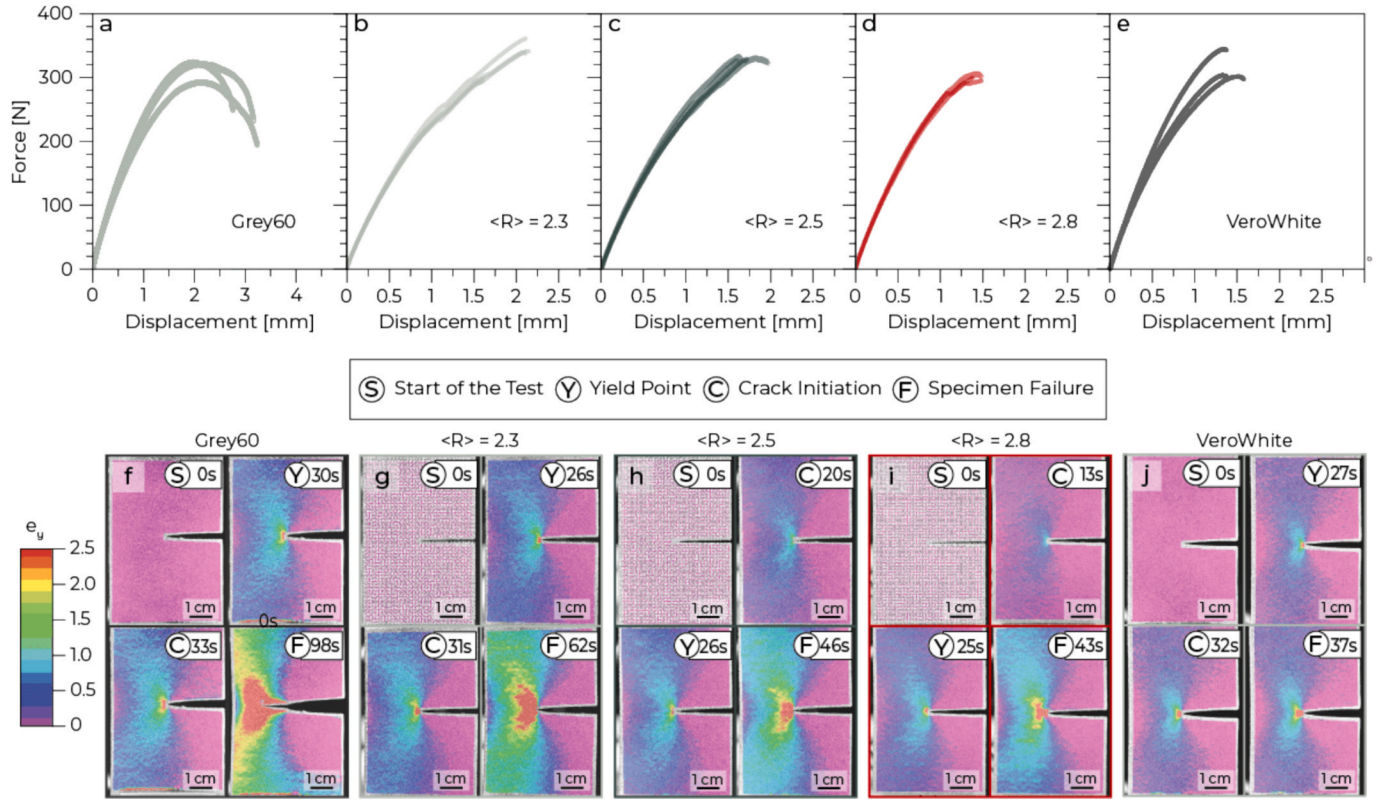
$$J = J_e + J_p \#$$

(2)

Fig. 2. Mechanical characterization and DIC images of plastic zone growth for bulk material and composite samples. (a-e) Force-displacement plots for bulk and composite samples. (f-j) 2D DIC strain maps of bulk and composite samples with plasticity threshold in red and time stamps.

$$J_e = \frac{\eta_e U_e}{Bb} \# \tag{3}$$

$$J_p = \frac{\eta_p U_p}{Bb} \# \tag{4}$$

where e and p refer to the elastic and plastic components, respectively (Anderson, 2017). By extracting the elastic and plastic components of the J-integral incrementally (Figure SI 3), we observe the tradeoff between recoverable and irrecoverable deformation within the samples, as the contribution to the normalized elastic J-integral increases as the coordination number increases, while the contribution to the normalized plastic J-integral decreases as the coordination number increases (Fig. 3c).

We then obtain the R-curves for each coordination by plotting the normalized J-integrals as a function of crack extension (Fig. 3d). Regardless of their coordination, all samples exhibit a rising trend, although the shape of each R-curve varies significantly across the coordination numbers (Fig. 3d). The 2.3 coordination samples have a higher critical J-integral value, J_c, at which the crack begins to grow, while the higher coordination samples show an average decrease in the critical J_c of 32.6 % and 61.2 % for 2.5 and 2.8 coordinations, respectively. After initiation, the 2.3 coordination samples all exhibit subcritical crack extension of a few characteristic lengths before reaching a saturation point, during which the crack arrests and the plastic zone grows until the sample reaches a maximum J-integral value, J_m, and the sample fails suddenly (Fig. 3d, left). In contrast, the 2.5 coordination samples all exhibit simultaneous crack extension and plastic zone growth before sample failure, reaching a 16.1 % lower average J_m than the 2.3 coordination samples (Fig. 3d, center). However, unlike the lower coordinations, the 2.8 coordination samples reach a saturation point in plastic zone size, allowing for several characteristic lengths of crack extension before sample failure, and reaching the lowest average J_m, 29.4 % lower than the 2.3 samples (Fig. 3d, right). We then

compare the composite materials with the bulk materials of the reinforcing and matrix phases. The bulk material of the matrix phase displays a larger plastic zone area than the 2.3 coordination samples and has a constantly rising R-curve with simultaneous crack extension. In contrast, the bulk material of the reinforcing phase displays a smaller plastic zone area than the 2.8 coordination samples, with a very short R-curve, as the sample fails at very low global strain with little crack extension (Figure SI 4).

3.3. Effect of structural features

Although the plastic zone size is the critical length scale to understand and describe the global fracture behavior (R-curves) of the samples, it is also necessary to consider a second length scale: the relative size and distribution of the structural features. Structural features are composed of groups of tiles which form different populations as a function of coordination number, resulting in plastic zone shape variations across the coordination numbers (Fig. 4a). Lower coordination numbers form more polydisperse structural features with a wide range of sizes, from one characteristic length squared up to tens of characteristic lengths squared, resulting in more extensible composite materials, while higher coordination numbers form more monodisperse structural features that are smaller, resulting in stiffer composite materials (Fig. 4a, SI 5).

In order to characterize the structural features, we describe their size in terms of their bridge lengths, defined as the distances between (T) tiles (Fig. 4b), and we note that the bridge lengths for each coordination are on the same order of magnitude as the characteristic length of 1 mm, which is at least one order of magnitude lower than that of the plastic zones (Fig. 4c). It is this relative size ratio, coupled with the reinforcing phase's higher strength, that results in a deformation which not only follows the shape of the local individual structural features ahead of the crack tip, but also globally the characteristic plastic zone shape from
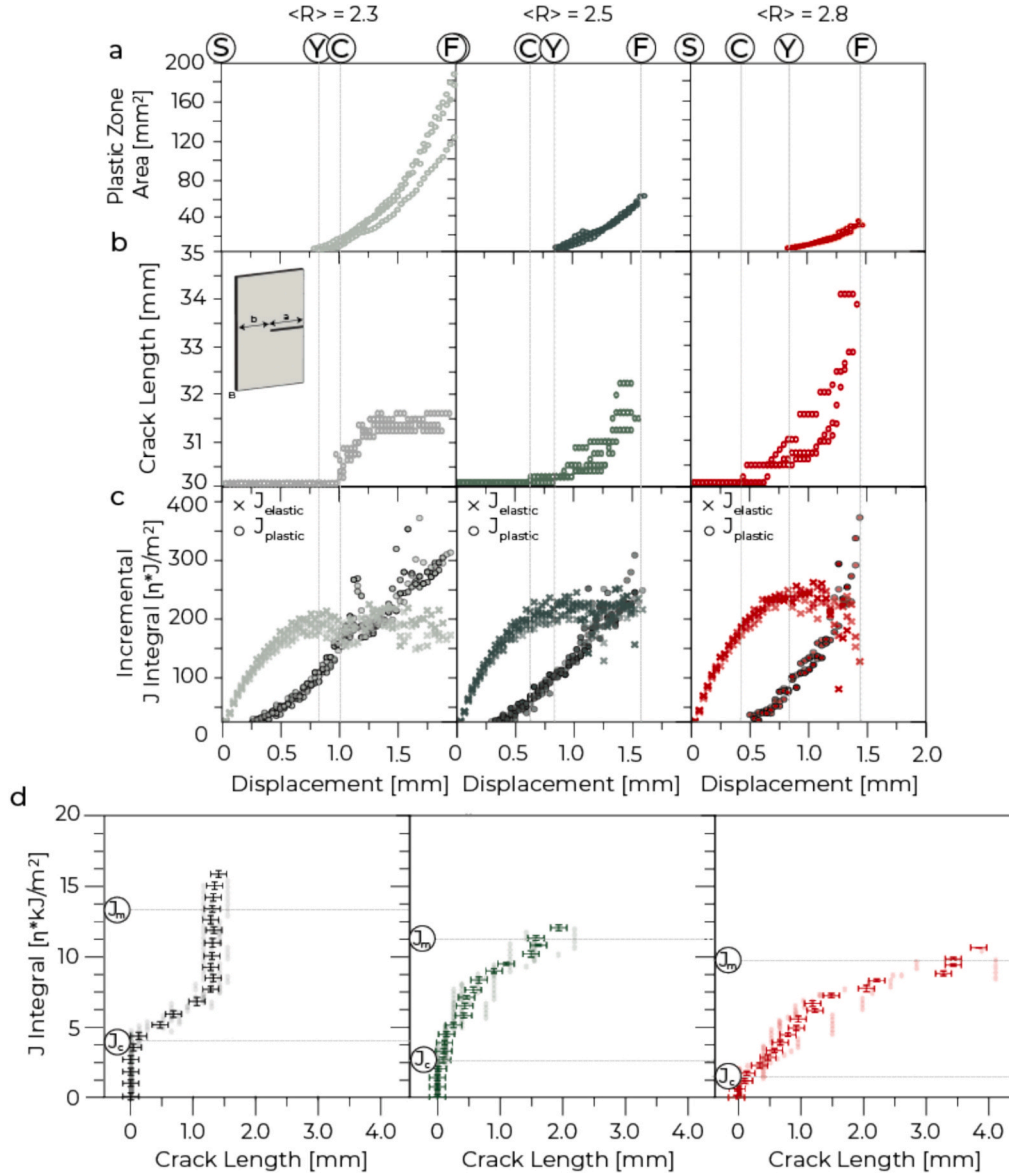
Fig. 3. Plastic zone size, crack extension length, J-integrals and R-curves for composite material samples. S corresponds to start of test, Y corresponds to yielding, C corresponds to crack initiation, F corresponds to failure. (a) Plastic zone area as a function of displacement for 2.3, 2.5, and 2.8 coordination samples. (b) Crack extension length as a function of displacement for 2.3, 2.5, and 2.8 coordination samples, with inset showing single edge notch plate tension sample dimensions. (c) Incremental elastic J-integrals (η_e normalized) and plastic J-integrals (η_p normalized) as a function of displacement for 2.3, 2.5, and 2.8 coordination samples. (d) R-curves for 2.3, 2.5, and 2.8 coordination samples.

linear elastic fracture mechanics (Anderson, 2017) (Fig. 4a).

Given that the strain field immediately ahead of the crack tip follows the shape of the local structural features (Fig. 4a), it is important to examine the orientation and geometry of these local features (Figs. 4d,e) to explain why higher coordination samples have greater crack extension. In order to generate higher coordination numbers, because they are stochastically generated on a square grid, samples are forced to form many smaller linear structural features that are aligned in the direction of the primary crack, at 0° (Fig. 4f). These linear features (Fig. 4e, red) can be more easily split apart, allowing for more crack extension at lower global strains. In contrast, lower coordination samples have fewer reinforcing interfaces to pass through than high coordination samples, and instead form many larger complex structural features that are at an angle to the primary crack, greater than 0° (Fig. 4f). It is more difficult for the crack to proceed through these extensible diagonal features (Fig. 4e, gray, green), resulting in crack arrest and allowing the sample to instead dissipate energy through the formation of a large plastic zone.

3.4. Plastic zone tailoring

With the two critical length scales in mind (the size of the plastic zone that is able to develop, and the population of structural features composing a given coordination number), we then seek to control the fracture response of the composite materials by spatially tailoring the coordination number. We create laminated assemblies with 25 % high coordination and 75 % low coordination regions in the sample (high-R edge) and then the inverse, with 25 % low coordination and 75 % high coordination regions (low-R edge) and perform the same single edge notch plate tension tests (Fig. 5a). We observe that the low-R edge makes it possible for the development of a significantly larger plastic zone in the 2.8 coordination region than the 100 % 2.8 coordination samples previously discussed (Figs. 5b,c). In contrast, the high-R edge prevents the formation of as large of a plastic zone in the 2.3 coordination region as observed in the 100 % 2.3 coordination samples previously discussed (Figs. 5b,d). This 'flipping' effect is likely the result of the similarity in
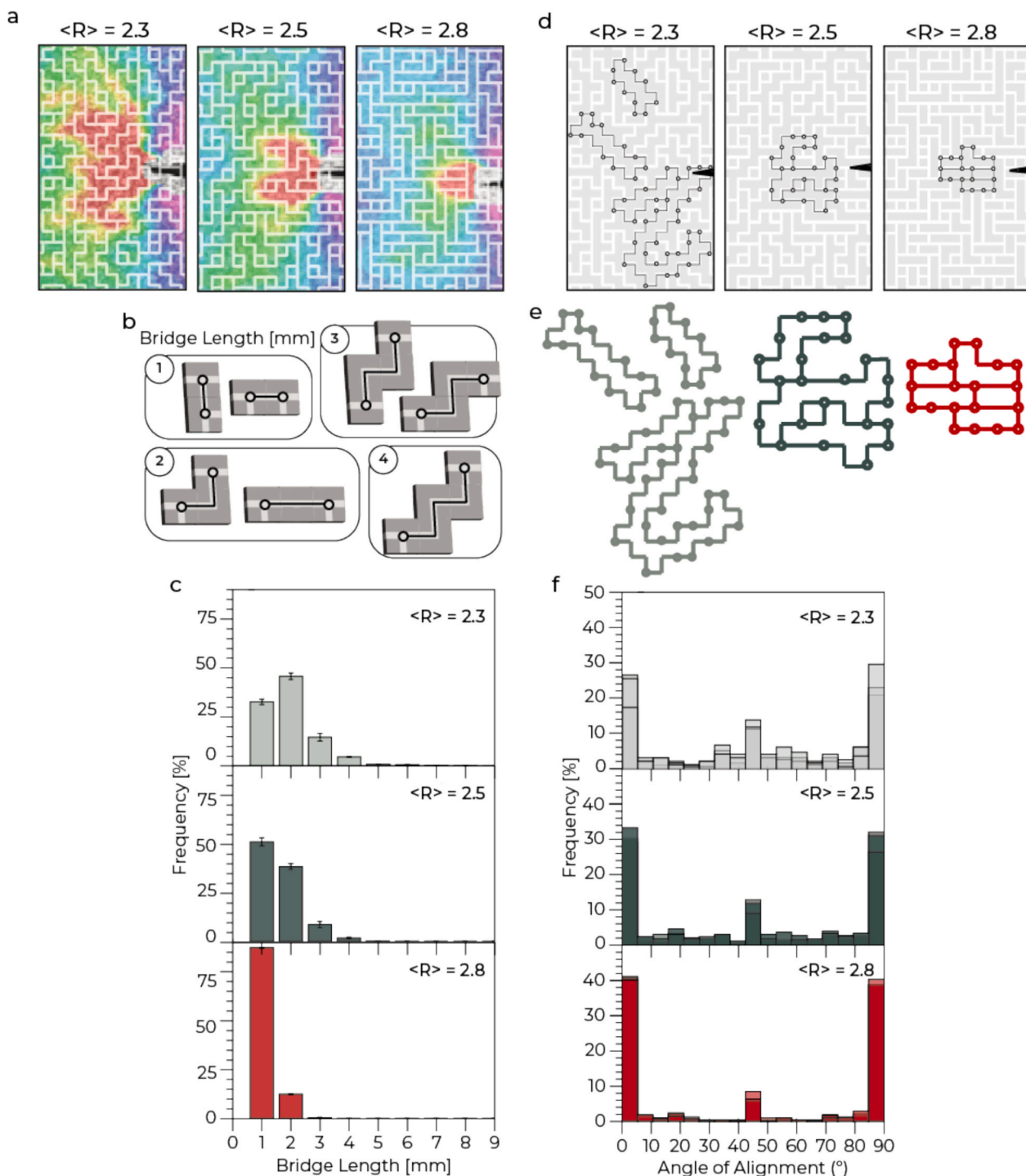
Fig. 4. Structural feature analysis. (a) Zoomed images of maximum plastic zone area for 2.3, 2.5, and 2.8 coordination samples with overlaid map of structural features. (b) Sample bridges for lengths of 1, 2, 3, and 4 mm (characteristic lengths). (c) Distributions of bridge lengths for 2.3, 2.5, and 2.8 coordination samples. (d) Samples with highlighted structural features ahead of the crack tip that contribute to the plastic zone shape for 2.3, 2.5, and 2.8 coordination samples. (e) Sample structural features with their constitutive bridges for 2.3, 2.5, and 2.8 coordination samples (gray, green, red, respectively). (f) Distributions of angles of alignment of structural features for 2.3, 2.5, and 2.8 coordination samples.

the matrix and reinforcing phase stiffnesses, which allows the entire structure to simultaneously engage in the deformation, prior to and during plastic zone formation. It is also important to note the effect of the interface where the low coordination region transitions to the high coordination region, and vice versa, which is only one characteristic length wide. This transition line causes the vertical flattening of the plastic zone in the high-R edge sample, as the population of structural features abruptly transitions from larger and more extensible to smaller

and less extensible (Fig. 5d). In contrast, the low-R edge sample transitions from smaller structural features to larger structural features, allowing for greater extensibility and a larger plastic zone ahead of the crack (Fig. 5c).

4. Conclusions

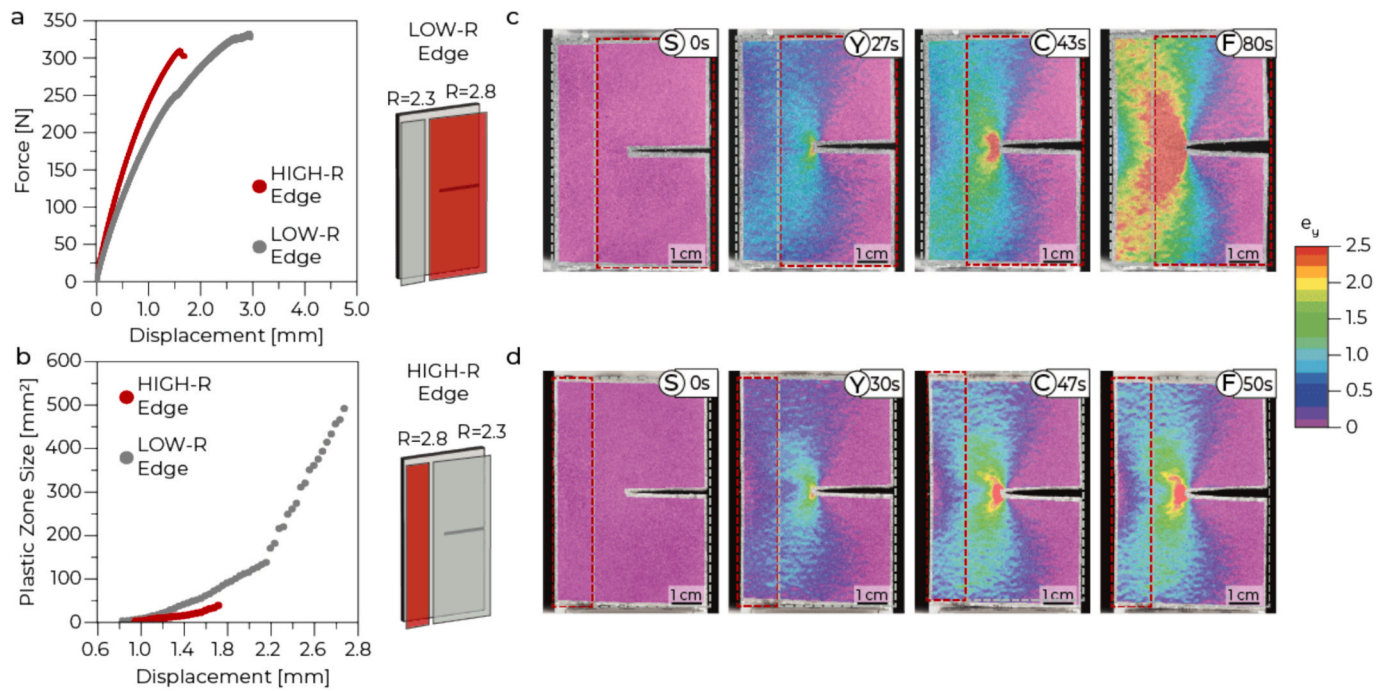We study the fracture behavior of nearly isodense polymer

Fig. 5. Tailoring the plastic zone. (a) 2.3 coordination and 2.8 coordination edge sample force–displacement plot. (b) Plastic zone size growth for 2.3 and 2.8 coordination edge sample. (c) 2D DIC strain maps for 2.3 coordination edge sample. (d) 2D DIC strain maps for 2.8 coordination edge sample.

composites with irregular network reinforcing phases and show how to tailor their fracture response. The composites feature a matrix phase with a similar stiffness but half the strength of the reinforcing phase, allowing for the formation and extension of a primary crack and therefore J-integral and R-curve measurements. We relate the effect of network coordination number, a global scale descriptor, to the mechanical properties of the reinforcing phase, through measurements of plastic zone size and crack extension. We observe that low coordination samples dissipate fracture energy through the formation of a large plastic zone, and fail at higher global strain, while high coordination samples dissipate energy through crack extension, and fail at lower global strain. We determine that there are two critical length scales that explain the fracture response of the polymer composites and the variations across the coordination numbers: (i) the size of the plastic zone, and (ii) the size and geometry of the structural features. Finally, we discuss how to tailor the tradeoff between plastic zone size and primary crack extension using the coordination number and its effect on the structural feature populations ahead of the crack tip.

CRediT authorship contribution statement

Chelsea Fox: Writing – review & editing, Writing – original draft, Visualization, Methodology, Investigation, Formal analysis, Data curation. **Tommaso Magrini:** Writing – review & editing, Writing – original draft, Supervision, Methodology, Conceptualization. **Chiara Daraio:** Writing – review & editing, Writing – original draft, Supervision, Funding acquisition, Conceptualization.

Declaration of competing interest

The authors declare that they have no known competing financial interests or personal relationships that could have appeared to influence the work reported in this paper.

Acknowledgements

The authors acknowledge F. Bouville and V. Vitelli for fruitful

Appendix A. Supplementary data

Supplementary data to this article can be found online at https://doi.org/10.1016/j.ijsolstr.2025.113658.

Data availability

Data will be made available on request.

References

Ackson, A.P.J., Vincent, J.F.V., Urner, R.M.T., 1988. The mechanical design of nacre. Proc. R. Soc. Lond. B Biol. Sci. 234, 415–440.

Anderson, T.L., 2017. Fracture Mechanics: Fundamentals and applications, Fourth Edition. Fundamentals and Applications, Fourth Edition, Fracture Mechanics, pp. 1–661.

Chen, C.H., Chang, R.R., Jeng, P.H., 1995. On the fiber-bridging of cracks in fiber-reinforced composites. Mech. Mater. 20, 165–181.

Dai, H., Dai, W., Hu, Z., Zhang, W., Zhang, G., Guo, R., 2023. Advanced composites inspired by biological structures and functions in nature: architecture design, strengthening mechanisms, and mechanical-functional responses. Adv. Sci. 10.

Dimas, L.S., Bratzel, G.H., Eylon, I., Buehler, M.J., 2013. Tough composites inspired by mineralized natural materials: Computation, 3D printing, and testing. Adv. Funct. Mater. 23, 4629–4638.

Dizon, J.R.C., Espera, A.H., Chen, Q., Advincula, R.C., 2018. Mechanical characterization of 3D-printed polymers. Addit. Manuf. 20, 44–67.

Espinosa, H.D., Rim, J.E., Barthelat, F., Buehler, M.J., 2009. Merger of structure and material in nacre and bone – Perspectives on de novo biomimetic materials. Prog. Mater Sci. 54, 1059–1100.

Fox, C., Chen, K., Antonini, M., Magrini, T., Daraio, C., 2024. Extracting geometry and topology of orange pericarps for the design of bioinspired energy absorbing materials. Adv. Mater. 2405567.

Gao, D., Chen, P., Lu, G., Yang, H., 2023. Numerical analysis for impact resistance of nacre-like composites. Mater. Today Commun. 35, 106031.

Gu, G.X., Libonati, F., Wettermark, S.D., Buehler, M.J., 2017a. Printing nature: Unraveling the role of nacre's mineral bridges. J. Mech. Behav. Biomed. Mater. 76, 135–144.

Gu, G.X., Su, I., Sharma, S., Voros, J.L., Qin, Z., Buehler, M.J., 2016. Three-dimensional-printing of bio-inspired composites. J. Biomech. Eng. 138, 0210061.

Gu, G.X., Takaffoli, M., Buehler, M.J., 2017b. Hierarchically enhanced impact resistance of bioinspired composites. Adv. Mater. 29, 1700060.

Jentzsch, M., Albiez, V., Kardamakis, T.C., Speck, T., 2024. Analysis of the peel structure of different Citrus spp. via light microscopy, SEM and µCT with manual and automatic segmentation. Soft Matter 20, 2804–2811.

Jentzsch, M., Becker, S., Thielen, M., Speck, T., 2022. Functional Anatomy, Impact Behavior and Energy Dissipation of the Peel of Citrus × limon: A Comparison of Citrus × limon and Citrus maxima. Plants 2022, Vol. 11, Page 991 11, 991.

Jia, Y., Liu, K., Zhang, X.S., 2024a. Unstructured growth of irregular architectures for optimized metastructures. J. Mech. Phys. Solids 192, 105787.

Jia, Y., Liu, K., Zhang, X.S., 2024b. Topology optimization of irregular multiscale structures with tunable responses using a virtual growth rule. Comput. Methods Appl. Mech. Eng. 425, 116864.

Jia, Z., Wang, L., 2019. 3D printing of biomimetic composites with improved fracture toughness. Acta Mater. 173, 61–73.

Jung, J., Chen, A., Gu, G.X., 2024. Aperiodicity is all you need: Aperiodic monotiles for high-performance composites. Mater. Today.

Keaveny, T.M., Morgan, E.F., Niebur, G.L., Yeh, O.C., 2003. Biomechanics of Trabecular. Bone. https://doi.org/10.1146/annurev.bioeng.3.1.307 3, 307-333.

Khan, R., 2019. Fiber bridging in composite laminates: a literature review. Compos. Struct. 229, 111418.

Kolednik, O., Predan, J., Fischer, F.D., Fratzl, P., 2014. Improvements of strength and fracture resistance by spatial material property variations. Acta Mater. 68, 279–294.

Launey, M.E., Buehler, M.J., Ritchie, R.O., 2010. On the mechanistic origins of toughness in bone. Annu. Rev. Mat. Res. 40, 25–53.

Li, F., Yu, C., Zhong, J., Zhao, C., 2024. Study on impact resistance of nacre biomimetic composite under interlamination functional gradient design. Mech. Adv. Mater. Struct.

Li, M., Zhao, N., Wang, M., Dai, X., Bai, H., 2022. Conch-Shell-inspired tough Ceramic. Adv. Funct. Mater.

Libonati, F., Colombo, C., Vergani, L., 2014. Design and characterization of a biomimetic composite inspired to human bone. Fatigue Fract. Eng. Mater. Struct. 37, 772–781.

Libonati, F., Vellwock, A.E., Ielmini, F., Abliz, D., Ziegmann, G., Vergani, L., 2019. Bone-inspired enhanced fracture toughness of de novo fiber reinforced composites. Scientific Reports 2019 9:1 9, 1–12.

Liu, K., Sun, R., Daraio, C., 2022. Growth rules for irregular architected materials with programmable properties. Science 1979 (377), 975–981.

Lumpe, T.S., Mueller, J., Shea, K., 2019. Tensile properties of multi-material interfaces in 3D printed parts. Mater. Des. 162, 1–9.

Magrini, T., Bouville, F., Lauria, A., Le Ferrand, H., Niebel, T.P., Studart, A.R., 2019. Transparent and tough bulk composites inspired by nacre. Nature Communications 2019 10:1 10, 1–10.

Magrini, T., Fox, C., Wihardja, A., Kolli, A., Daraio, C., 2023. Control of Mechanical and Fracture Properties in Two-Phase Materials Reinforced by Continuous. Irregular Networks, Advanced Materials.

Magrini, T., Libanori, R., Kan, A., Studart, A.R., 2021. Complex materials: the tough life of bone. Revista Brasileira De Ensino De Fisica 43, 1–17.

Magrini, T., Senol, A., Style, R., Bouville, F., Studart, A.R., 2022. Fracture of hierarchical multi-layered bioinspired composites. J. Mech. Phys. Solids 159, 104750.

Metzler, R.A., Barthelat, F., Wilker, J.J., 2019. Disordered structures in biology can provide material properties not obtained with precise hierarchy. Adv. Funct. Mater. 29, 1805734.

Meyers, M.A., Lin, A.Y.M., Chen, P.Y., Muyco, J., 2008. Mechanical strength of abalone nacre: Role of the soft organic layer. J. Mech. Behav. Biomed. Mater. 1, 76–85.

Nash, R.J., Li, Y., 2021. Experimental and numerical analysis of 3D printed suture joints under shearing load. Eng. Fract. Mech. 253, 107912.

Nemat-Nasser, S., Hori, M., 1987. Toughening by partial or full bridging of cracks in ceramics and fiber reinforced composites. Mech. Mater. 6, 245–269.

Rigidity Theory and Applications, 2002. Rigidity Theory and Applications.

Sakai, M., Miyajima, T., Inagaki, M., 1991. Fracture toughness and fiber bridging of carbon fiber reinforced carbon composites. Compos. Sci. Technol. 40, 231–250.

Schneider, C.A., Rasband, W.S., Eliceiri, K.W., 2012. NIH Image to ImageJ: 25 years of image analysis. Nature Methods 2012 9:7 9, 671–675.

Slesarenko, V., Rudykh, S., 2018. Towards mechanical characterization of soft digital materials for multimaterial 3D-printing. Int. J. Eng. Sci. 123, 62–72.

Studart, A.R., 2012. Towards High-Performance Bioinspired Composites. Adv. Mater. 24, 5024–5044.

Thorpe, M., Duxbury, P., 2002. Rigidity theory and applications. Rigidity Theory and Applications.

Thorpe, M.F., 1983. Continuous deformations in random networks. J. Non Cryst. Solids 57, 355–370.

Whitehouse, W.J., 1974. The quantitative morphology of anisotropic trabecular bone. J. Microsc. 101, 153–168.

Zhang, Y., Hsieh, M.T., Valdevit, L., 2021. Mechanical performance of 3D printed interpenetrating phase composites with spinodal topologies. Compos. Struct. 263, 113693.

Zhou, Y.H., Zheng, Y.F., Zhang, Y.Q., Wu, H.A., Liu, C., 2024. Inverse design of growth-inspired irregular architected materials for programmable properties. Extreme Mech. Lett. 70, 102196.

Zhuang, Z., Qian, Z., Wang, X., Xu, X., Chen, B., Song, G., Liu, X., Ren, L., Ren, L., 2023. Bioinspired Structural Composite Flexible Material with High Cushion Performance. Advanced Science.